Research Article | Vol. 11, No. 1 / 1 January 2021 / Optical Materials Express 59
Optical Materials EXPRESS

L-band femtosecond fiber laser based on a reduced graphene oxide polymer composite saturable absorber

E. K. NG,[1] K. Y. LAU,[2] H. K. LEE,[3] N. MOHD YUSOFF,[1] A. R. SARMANI,[4] M. F. OMAR,[5] AND M. A. MAHDI[1,*]

[1]*Wireless and Photonics Networks Research Centre, Faculty of Engineering, Universiti Putra Malaysia, 43400 UPM Serdang, Selangor, Malaysia*
[2]*Department of Electronics and Nanoengineering, Aalto University, Espoo 02150, Finland*
[3]*Department of Electronic Engineering, Faculty of Engineering and Green Technology, Universiti Tunku Abdul Rahman, 31900, Kampar, Perak, Malaysia*
[4]*Department of Physics, Faculty of Science, Universiti Putra Malaysia, 43400 UPM Serdang, Selangor, Malaysia*
[5]*Physics Department, Faculty of Science, Universiti Teknologi Malaysia, 81310 Skudai, Johor, Malaysia*
[*]*mam@upm.edu.my*

Abstract: We demonstrate an L-band passively mode-locked erbium-doped fiber laser emitting at 1599.43 nm wavelength at a pulse train of 5.68 MHz. The microfiber reduced graphene oxide composite behaves as a saturable absorber that was fabricated using in-situ wet chemical and dip-coating methods. During operation, a single-pulse soliton was observed at a mode-locking threshold of 40 mW. This is a few times lower than most of the previous assessments in the same class of wavelength band and graphene saturable absorbers. The pulse duration was 568 fs with a maximum average output power of 6.75 mW. In addition, the superiority of this simple fabrication method facilitates its potential of mass production for applications in ultrafast photonics industries.

1. Introduction

Ultrafast lasers have been a popular research topic due to their distinguished advantages in a number of science and technology areas [1–2]. To extend beyond the limit of C-band telecommunication window [3,4], these lasers particularly at L-band wavelengths (1565-1625 nm) are developed. They have many applications in supercontinuum generation [5], gas spectroscopy [6], biomedical science [7], three-photon microscopy [8], and optical communications due to their high repetition rate [9]. To date, ultrashort pulses in this region can be realized through either active or passive mode-locking techniques.

One of the simplest methods is incorporating an external electro-optic modulator (EOM) into a laser cavity to achieve short pulses (ns-ps) at 1600 nm waves [10]. However, the EOM is bulky and has restricted responses with requirements of external electrical components that could induce difficulty in generating femtosecond lasers. On the contrary, passive mode-locking is achieved through the third order nonlinearity when a high intensity light passes through the optical fiber with a small core diameter ~8 μm for a single mode fiber. A material that was incorporated upon the passage of this light is dubbed as a saturable absorber (SA). Upon its discovery, various extensive developments in mode-locking properties are attained such as power, operating wavelength, pulse width, repetition rate and laser stability.

During early days, a semiconductor saturable absorber mirror (SESAM) has been the traditional component to achieve passive mode-locking in fiber lasers [11]. Nonetheless, it has several drawbacks on operating bandwidth, long recovery time of more than 1 ps and complex micro-fabrication process. Apart from SESAM, recent studies on other SA fabrication based on

#404238 https://doi.org/10.1364/OME.404238
Journal © 2021 Received 31 Jul 2020; revised 16 Sep 2020; accepted 17 Sep 2020; published 8 Dec 2020

Optical Materials EXPRESS

rare-earth materials have been reported. The carbon nanotube (CNT) SA is among the first nanomaterials that can be integrated into all-fiber devices. These include by directly sandwiching between two-fiber ends [12], optical deposition on microfibers [13], or the side polished fibers [14]. Despite its success, the CNT SA operation wavelength depends on the diameter and chirality of the tube which limits its potential for broadband coverage. Alternatively, materials such as graphene, topological isolators, transition metal dichalcogenides, black phosphorus, and MXene based SAs have been successfully demonstrated for ultrashort pulse generation from near to mid-infrared region [15–16].

Among these SAs, graphene can be easily synthesized using well-known fabrication techniques including mechanical exfoliation [17], molecular beam epitaxy (MBE) growth [18], chemical exfoliation [19], and chemical vapor deposition (CVD) [20]. Other materials are much more complicated to synthesize which require excellent knowledge of material sciences. In most of recent studies, the graphene was typically deposited between fiber ferrule structures [21–22]. As a result of very small fiber core diameter, the highly concentrated power is focused on the limited interaction surface area of this structure. This could result in thermal damage when operating at high pump power. A promising solution to this issue is to have lateral interaction of graphene-based materials with propagated evanescent waves along the optical fibers [23–24].

In this work, we demonstrate the fabrication and employment of reduced graphene oxide/polydimethylsiloxane (rGO/PDMS) coated microfiber as a SA. An L-band ultrashort pulse operation in the erbium-doped fiber laser cavity at 1599.43 nm center wavelength was attained with a pulse duration of 568 fs. The advantages of this technique lie within the readily commercialized rGO in the market, combining with the polymer that supports mechanical structures of the tapered fiber. These robustness and practicality make the ultrafast laser sources as the potential candidates in the molecular spectroscopy, nonlinear frequency conversion as well as laser surgery applications.

2. Materials and methods

2.1. Fabrication of the rGO polymer composite

The raw materials namely rGO, isopropyl alcohol (IPA, 99.5%) and PDMS (Sylgard 184 Silicone Elastomer) were used as received originally without having further purifications. The rGO was obtained from ACS Material LLC, USA and the IPA were procured from Sigma Aldrich. On the other hand, the polymer was purchased from Dow Corning. The fabrication scheme involves in-situ wet chemical for material preparations (see Fig. 1), microfiber tapering and dip-coating (see Fig. 2). This begun in Fig. 1(a to f) by dispersing 0.8 mg of rGO powders in 10 ml of IPA through an ultrasonic probe (Hielscher UP200s) for 1 hour. After sonication, 1.0 g of polymer (PDMS) was added to the homogenous rGO solution. This was heated at 80 °C for 16 hours with continuous stirring at ~200 rpm to ensure complete evaporation of the solvent. This step is crucial to allow a solid formation of rGO/PDMS composite. Next, 0.1 g of curing agent was added into the mixture and stirred for 10 minutes. In order to remove bubbles from the mixture, a degassing process was carried out in the vacuum oven (CONSTANCE VC-6050) for half an hour duration.

For microfiber tapering, a single mode fiber (SMF-28) was stripped of its coating polymer (3 cm length) before putting onto a glass processing workstation (Vytran GPX-3000) stage holders. The taper properties are shown in Fig. 2(a) with a waist diameter of 10 μm, a waist length of 1 mm and a taper transition of 30 mm. These parameters provided the adiabaticity with tapering loss of less than 0.3 dB while sustaining the large evanescence interaction length. The heat source can be precisely controlled using the built-in software to achieve the desirable microfiber diameter. After the tapering process, the microfiber was coated with the finished product of rGO/PDMS composite through dipping method for 20 seconds as illustrated in Fig. 2(b). Then, the microfiber

Optical Materials EXPRESS

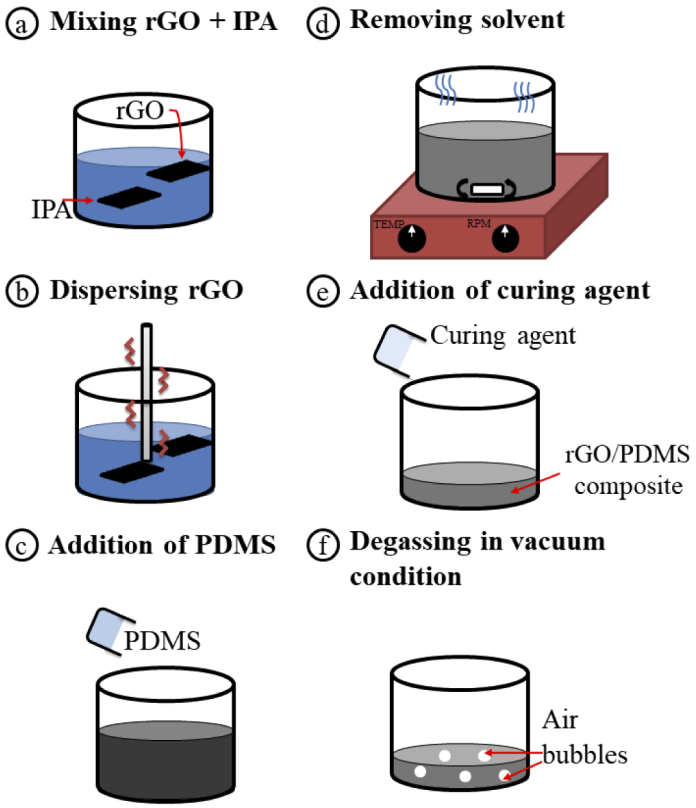

Fig. 1. Preparation procedures, (a) mixing rGO with IPA, (b) dispersing rGO, (c) addition of PDMS, (d) removing solvent, (e) addition of curing agent and (f) degassing in vacuum condition.

was fixed on a grooved sample holder with epoxy glue as shown in Fig. 2(c). For curing process that hardens and stabilizes the composite, this stand was left in a dry cabinet for 24 hours period.

2.2. *Characterization of materials and saturable absorption properties*

The material characterization comprises morphological and spectroscopic studies of the rGO/PDMS composite and its constituents as presented in Fig. 3, Fig. 4, and Fig. 5. Once these insights are comprehended, optical properties of the mode-locking device were assessed as elucidated in Fig. 6. Initially, the Field Emission Scanning Electron Microscope (FESEM-Hitachi SU8000) was set at an accelerating voltage of 2 kV and a working distance of 3.7 nm with 10000x magnification. It can be observed from Fig. 3(a) that the rGO sheets are overlapped and folded (wrinkled sheet) due to sample preparation when placing the powder on the aluminium stab holder. For performing UV-Visible diffuse reflectance (Shimadzu UV3600), the material was dispersed in water for absorption evaluation. Maximum absorption at ~260 nm was observed, resulting from partial restoration π-π^* transition of aromatic C-C bonds. This peak is deemed to be the reduction of GO as shown in Fig. 3(b) [25]. Besides this, Raman spectroscopy was implemented by utilizing Horiba Scientific - LabRAM HR Evolution. Several peaks at D band (1351.39 cm^{-1}), G band (1595.49 cm^{-1}), 2D band (2713.94 cm^{-1}) and D + G band (2919.49 cm^{-1}) are shown in Fig. 3(c). The reduction degree typifies the ratio between intensity of D band to that of G band. From these findings, the ratio was 0.84 where it has more C = C bonding (sp^2

Optical Materials EXPRESS

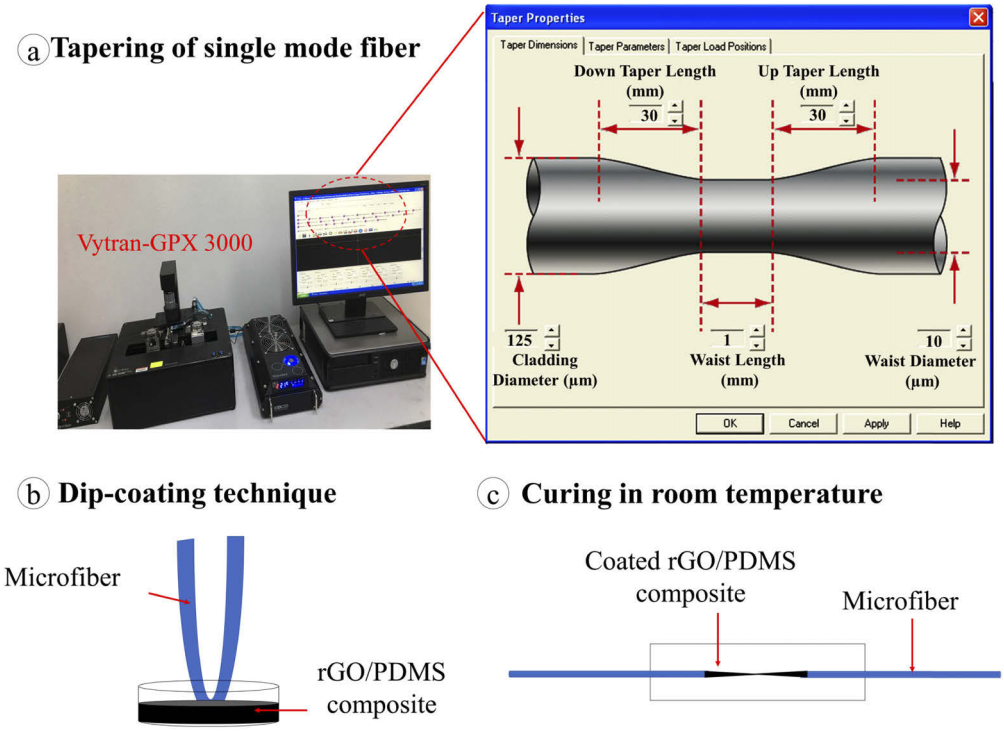

Fig. 2. Deposition processes (a) tapering of single-mode fiber, (b) dip-coating of rGO/PDMS composite on the microfiber and (c) sample curing at room temperature.

hybridization) than C-C bonding (sp^3 hybridization) that validated the presence of rGO in the prepared sample.

Figure 4 describes Raman intensity (under 532 nm excitation) for the cured rGO/PDMS composite coated microfiber (black line) together with the inset visual at the scale bar of 200 µm. For comparison, other features for PDMS polymer (blue line) and a single data for the rGO powder (red line) which is similar to that presented in Fig. 3(c) are also included. The diagram ascertains the actual composition of the composite. There were obvious peaks specifically at 2895.48 cm^{-1} and 2960.75 cm^{-1} for the black line in agreement to the spectral profile of the blue line. In addition, the peaks at 1351.39 cm^{-1} and 1595.49 cm^{-1} for the black line also correspond to the D-band and the-G band Raman peaks for the red line.

The following steps are focused mainly on the composite material. To conduct FESEM and energy dispersive X-ray (EDX) analysis as shown in Fig. 5, Zeiss Crossbeam 340 and Oxford Silicon Drift Detector X-Max systems were utilized, respectively. Figure 5(a) depicts the back-scattered FESEM image, the microfiber has unavoidable thick accumulation of composite at its bottom as a result of dip coating (see Fig. 8 in [26]). Meanwhile, Fig. 5(b-d) with different color mapping denotes the existence of oxygen (O), silicone (Si), and carbon (C) which were uniformly distributed. The corresponding weight percentage, wt% can be evaluated from Fig. 5(e) where the visible red spot in the inset of this figure signifies the precise location where this EDX data was acquired. In this case, 58.1 wt% for Si, 24.5 wt% of C and 17.4 wt% of O verify the ingredients of rGO/PDMS which coincide well to the Raman analysis.

Before proceeding with testing the functionality of the mode-locking device, the saturable absorption attributes were analyzed first using the arrangement as illustrated in Fig. 6(a). From this figure, a Menlo Systems M-Fiber pulsed laser source (1560 nm, 117 fs, and 250 MHz) was

Optical Materials EXPRESS

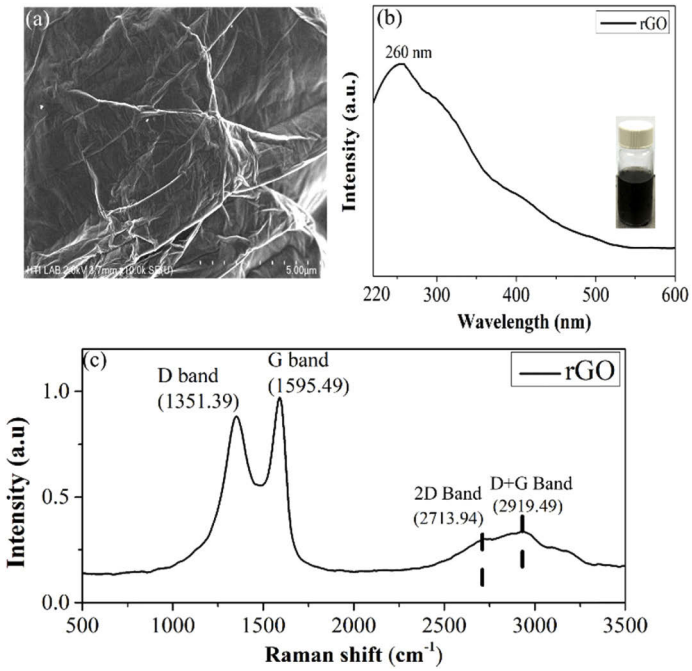

Fig. 3. Scientific structures of rGO, (a) a FESEM image, (b) UV-VIS absorption and (c) Raman spectra.

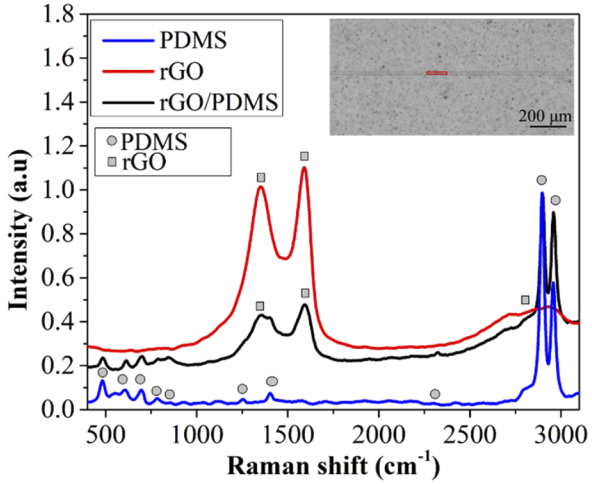

Fig. 4. Raman transitions in rGO, PDMS and its composite as well as (inset) the microscope image of the composite.

Optical Materials EXPRESS

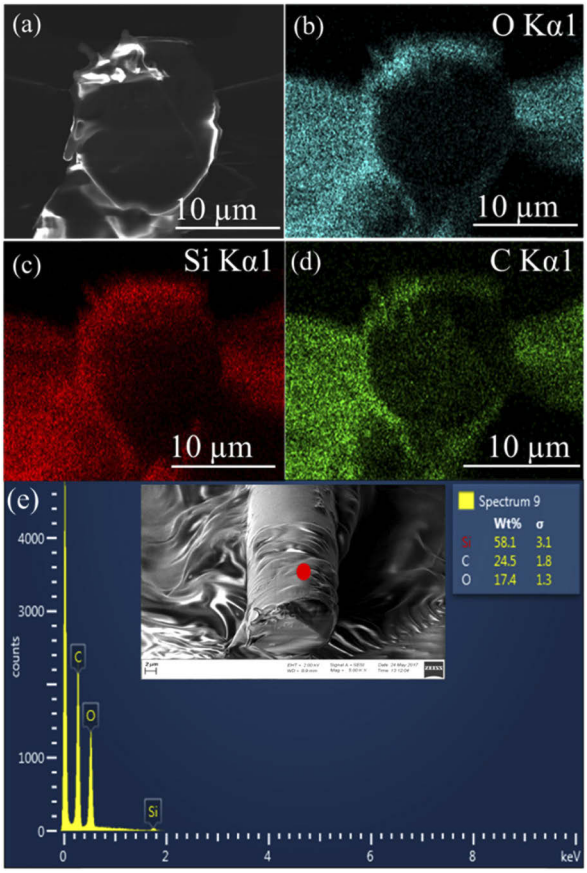

Fig. 5. Morphology of rGO/PDMS composite coated microfiber, (a) a FESEM cross-section, (b) EDX colors representation for O, (c) Si and (d) C where (e) EDX spectra with (inset) the microfiber close-up.

coupled to a variable optical attenuator (VOA). The 50:50 ratio optical coupler was employed to divide the optical pulse source into two equal portions. One leg was used as a source of reference to monitor the input power via an optical power meter (OPM1) while another leg was terminated by OPM2 to measure the output optical power after passing through the SA. In this experiment, both powers were measured simultaneously where the data are then fitted according to the formula [27];

$$T(I) = 1 - \alpha_{ns} - \Delta T \times \left[\exp\left(-\frac{I}{I_{sat}}\right)\right] \tag{1}$$

where $T(I)$ is the transmission rate, α_{ns} is the non-saturable absorbance, ΔT is the modulation depth, I is the input intensity of laser, and I_{sat} is the saturation intensity. In our experiment, the α_{ns} was 39.10%, the I_{sat} and ΔT were assessed to be 60 MW/cm^2 and 3.9%, respectively. The latter value is comparable to other reports in the same topics of graphene that vary from less than 1% up to 5.5% [26,28–30]. However, the saturable absorption is limited by the dip coating method used in this work. It is believed that the saturable absorption properties can be further optimized by controlling the thickness of two-dimensional materials via spin coating method as previously reported in [31–32].

Optical Materials EXPRESS

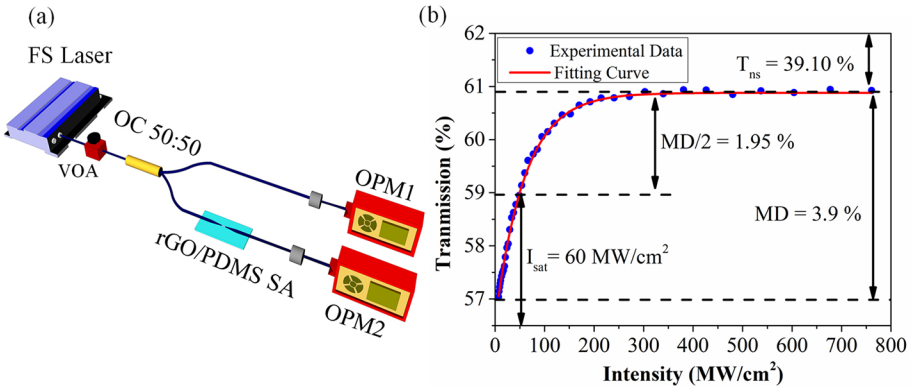

Fig. 6. (a) Twin detector measurement setup and (b) nonlinear responses of the SA.

2.3. *Laser cavity setup*

The schematic diagram of the fiber laser that consisted of 20 m length SMF-28 is portrayed in Fig. 7. A 1480 nm laser diode (LD) was used as a pump source instead of that at 980 nm in order to increase the power conversion efficiency [33].The gain medium was a section of 17 m long erbium-doped fiber (EDF-Liekki Er80-8/125) that was connected through a 1480/1550 nm wavelength division multiplexer (WDM). The EDF fiber has a mode field diameter of 9.5 µm, a numerical aperture of 0.13 and a cutoff wavelength at 1250 nm. It has an absorption coefficient of 80 dB/m at 1530 nm wavelength where this highly doping concentration is required owing to the low gain coefficient in the L-band [34]. The dispersion coefficients of the EDF and SMF-28 were 15.7 ps/nm/km and 17 ps/nm/km, respectively. These result in the estimated total net anomalous dispersion of -0.823 ps^2. Besides this, a polarization independent isolator (ISO) was employed to ensure unidirectional light propagation in a clockwise direction. The rGO/PDMS composite coated microfiber (SA) that starts the formation and stabilization of ultrashort pulses was spliced in between the ISO and optical coupler (OC). The output laser signal was extracted via a 30% of OC, whereas the remaining laser signal (70%) propagated in the cavity towards the polarization controller (PC). The PC controls the birefringence inside the single-mode fiber and further assists the initiation of ultrashort pulses in its optimized polarization angle.

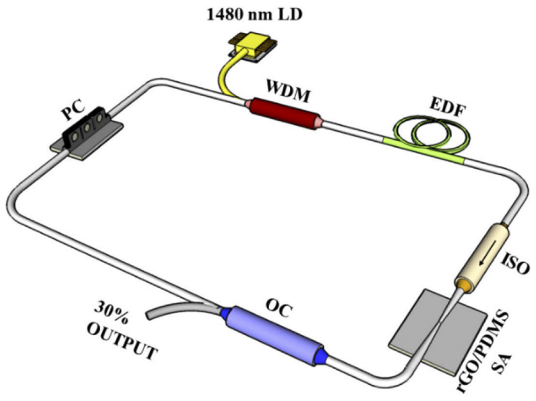

Fig. 7. L-band passively mode-locked erbium-doped fiber laser (EDFL) employing rGO/PDMS SA.

Optical Materials EXPRESS

3. Results and discussions

At the outset of this assessment, the lasing behaviors in Fig. 8(a) were investigated while maintaining the PC at the optimized polarization state. From this figure, the pump power (P_p) was restricted to a maximum of 166 mW to prevent any damage to the SA. Once lasing was started, the mode-locking threshold was firstly achieved at P_p of 40 mW as signified by immediate broadening in the spectral width. This is reasonable when comparing to other attainments of 31 mW in [35] and nearly 92 mW in [36]. Above this level, ultrashort pulses remained viable where maximum output power of 6.75 mW was satisfied. The slope efficiency determined from the linear red line curve was 5.3%. Furthermore, the pulse energy (E_p) grew from 0.04 to 1.19 nJ as demonstrated by the blue plot. In fact, this criterion was deduced by multiplying the average output power to that of the cavity round trip time, $P_{out} \times T_{rt}$. The T_{rt} of 176 ns was measured by an oscilloscope at the maximum power level [see Fig. 8(b)]. This corresponds to the cavity length of 37 m built in this report.

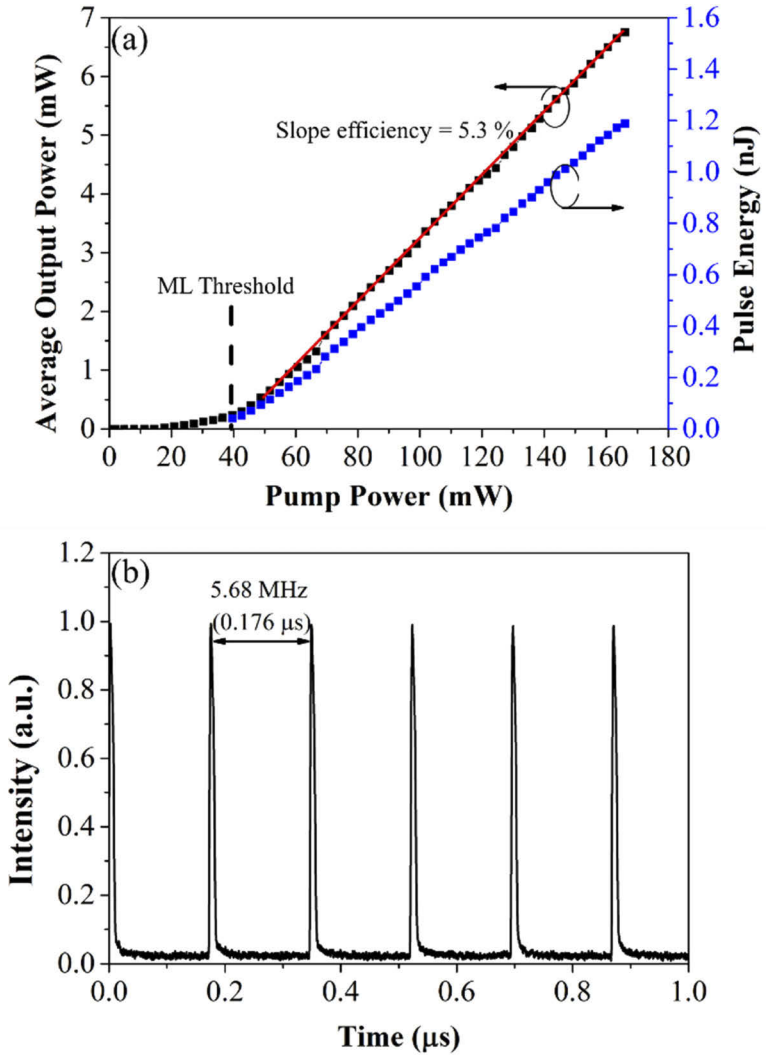

Fig. 8. (a) Average output power (black colour) and pulse energy (blue colour) against the pump power and (b) the oscilloscope pulse train at P_p = 166 mW.

Optical Materials EXPRESS

Figure 9(a) illustrates the evolution of ultrashort pulses against the pump power for every 3 mW interval. The peak intensity together with 3-dB bandwidth enhanced proportionally at higher pump power. The image justifies no presence of parasitic continuous wave lasing component. A few selected results at just below and at mode-locking thresholds as well as at maximum P_p that relate to Fig. 8(a) are shown in the inset of Fig. 9(b). The broader bandwidth with the sign of Kelly sidebands as represented by the red and blue profiles indicate a typical soliton pulse shaping scheme [37]. Notably, no noise like spike existed in the mode-locked spectrum at maximum pump power as manifested by the primary signal in Fig. 9(b). In this case, the central wavelength and spectral width were measured to be 1599.43 nm and 5.71 nm, respectively.

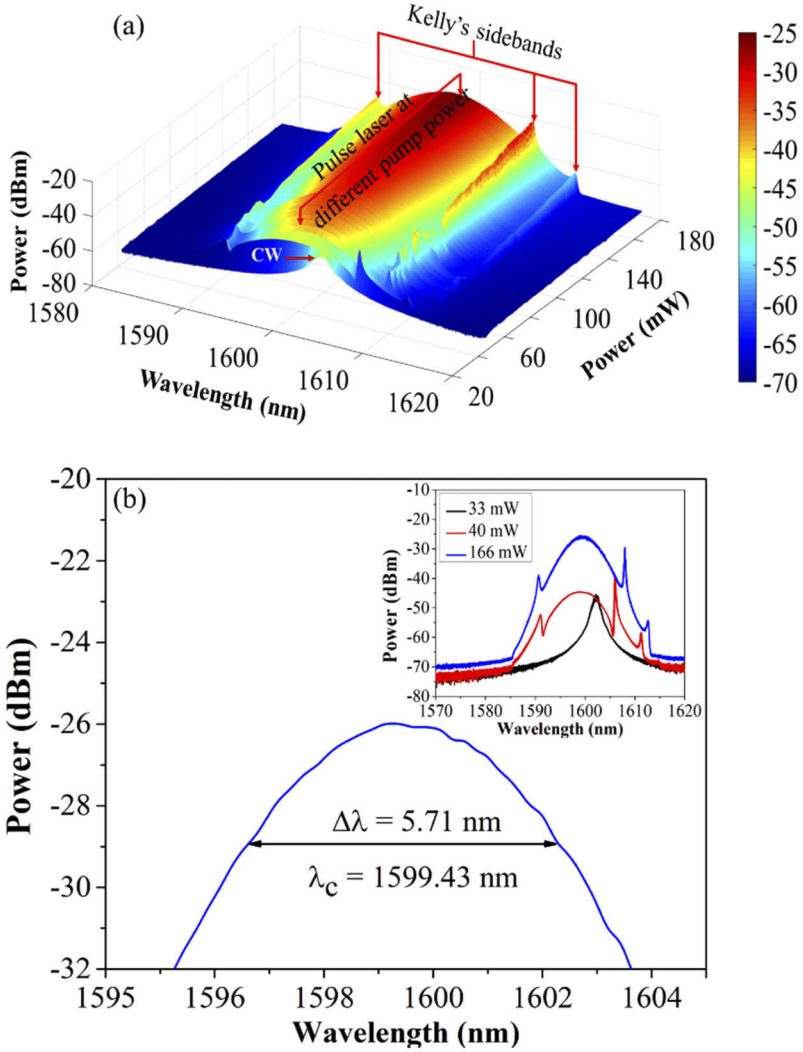

Fig. 9. Progress of L-band curves, (a) 3D images, (b) 2D images with the enlarged soliton pulse at P_p of 166 mW and (inset) a few chosen results.

The measured spectral width of 5.71 nm corresponds to the autocorrelation full width at half maximum (FWHM) of 874.72 fs. By assuming a perfect sech^2 fitted curve as validated in Fig. 10(a), the actual pulse width after considering a deconvolution factor of 1.543 was determined to be 568 fs. Due to residual chirp, the time bandwidth product was 0.38 which

Optical Materials EXPRESS

is slightly higher than the ideal transform limited value of 0.315. In addition to this, the radio frequency (RF) spectrum measured by an electrical spectrum analyzer (ESA) at a maximum power level has an excellent signal to noise ratio of 59.5 dB as proven in Fig. 10(b). The inset in this figure with high-order harmonics generation within 50 MHz frequency domain that pertains to Fig. 8(b) ascertains no observable sign of Q switching instabilities [38]. In addition, as the recorded pulses retain similar separation that implies no pulse breaking was initiated in the laser cavity.

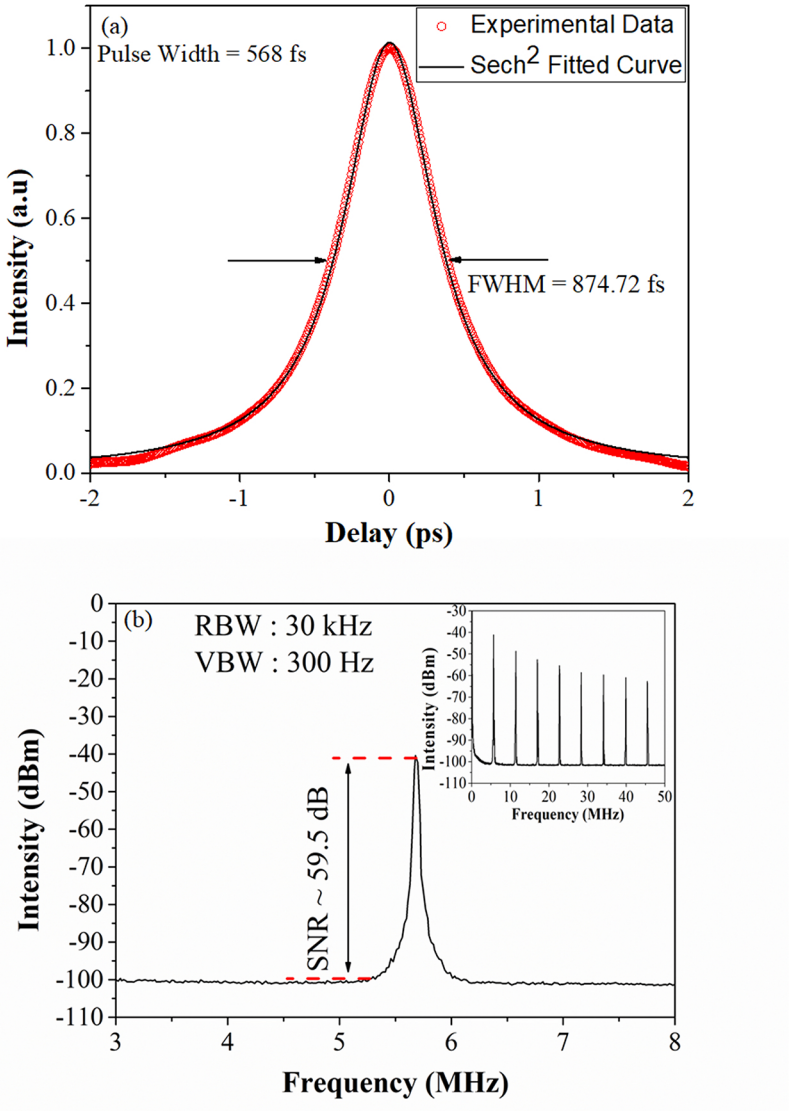

Fig. 10. Signals at P_p of 166 mW, (a) autocorrelation trace, (b) the RF spectrum and (inset) high-order harmonics at 50 MHz span of the ESA.

To confirm the reliability and robustness of the SA to sustain mode-locking operation, stability tests at constant polarization state and maximum pump power were carried out as outlined in Fig. 11. For over 1-hour duration with 2 minutes interval, the measured spectral images are

Optical Materials EXPRESS

depicted in Fig. 11(a) where more details are given in Fig. 11(b). From the bottom diagram, the average central wavelength prevailed at 1599.39 ± 0.04 nm. Concurrently, the spectral bandwidth also remained at 5.71 nm with minimum fluctuations of ± 0.04 nm throughout the same time period. These justify the favorable properties of the fabricated SA in producing femtosecond pulses that can satisfy the industrial and scientific demands. Amongst their applications include micromachining, femtochemistry, optical communication, frequency comb and etc.

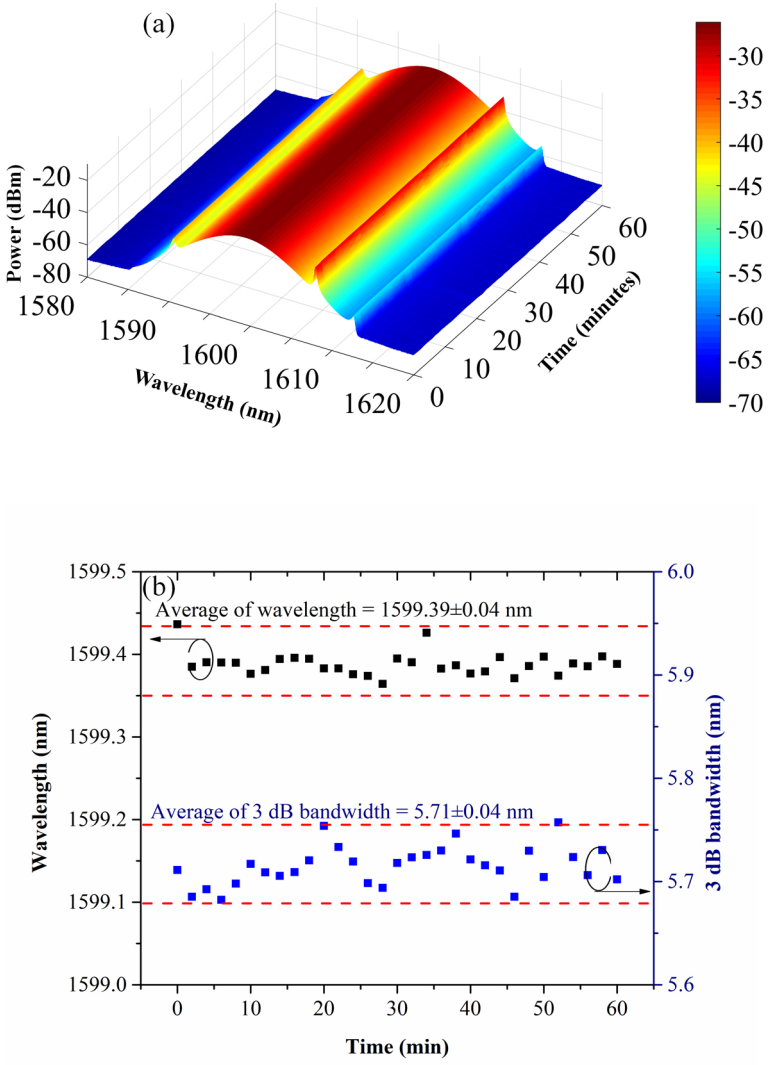

Fig. 11. Stability tests at P_p of 166 mW over 1 hour, (a) spectrogram and (b) center wavelength and its 3 dB bandwidth.

Other earlier developments in the same category are summarized in Table 1, mostly involving sandwiching graphene films between fiber ferrules. This integration method is well known for having a low damage threshold which is not feasible for high power operation. A better solution that incorporated the rGO film on the D-shaped fiber resulted in a similar mode-locked threshold but with much shorter pulses compared to our results [39]. The contributing factors relate to the optimized intracavity dispersion and additional external compression of the stretched-soliton

Optical Materials EXPRESS

pulse. Despite of these benefits, the fundamental mode-locked laser has short term stability within 15 minutes range only. In addition, the polishing of the D-shaped fiber often induces uncontrollable inhomogeneity that necessitates high technical expertise. This requirement was eliminated by the favorable choice of implementing microfiber that brings together the advantage of controllable fabrication process. Very stable soliton pulses generation with the presence of Kelly sidebands are presented in our work. With the exploitation of evanescent field interaction, the issue of thermal damage was also resolved. Much lower mode-locked threshold was satisfied than those in [21,22,36,40] with comparable pulses to other reported literatures [21,22,36]. Up to date, graphene-polymer composites-based SA in L-band using microfiber have yet to be thoroughly explored. In the future, we expect the direction of this work towards power scaling attempts.

Table 1. Progresses in SA for ultrafast EDFLs at L-band.

Ref.	Implementation	Center wavelength (nm)	Maximum pulse energy (nJ)	Pulse width (fs)	Mode-locked threshold (mW)
21	Sandwiching atomic graphene thin film between fiber ferules	1576.30	7.30	415	130
22	Sandwiching graphene oxide/polyvinylalcohol film between fiber ferules	1595.84	0.04	426	108
36	Sandwiching graphene/tungsten disulfide heterostructure film between fiber ferules	1601.90	0.23	660	92
39	D-shaped optical fiber with the rGO film SA	1566.00	0.08	190	40
40	Sandwiching graphene oxide saturable on fluorine mica substrate between fiber ferules	1567.29	1.44	1380000	273
This work	Dip-coating the rGO/PDMS composite around the tapered region of the microfiber on a groove	1599.43	1.19	568	40

4. Conclusion

In summary, we have successfully demonstrated the ease of fabricating the rGO/PDMS composite in the laboratory. Its precise O, C and Si contents that differ from 17% to 58% were obtained from the morphological and spectroscopic studies. This material served as a saturable absorber in an ultrafast EDFL by initiating lateral interaction with propagated evanescent waves along the tapered microfiber. During operation, a pulse duration of 568 fs was initiated at the central wavelength of 1599.43 nm. This work on microfiber-based SA in the L-band satisfies the expansion requirement of the telecommunication window. Further supporting evidence of stable laser output over an observation period of 60 minutes and low threshold operation display the potentials in developing this technology at cost efficient upgrade.

Funding

Ministry of Higher Education, Malaysia (FRGS/1/2017/TK04/UPM/01/2).

Disclosures

The authors declare no conflicts of interest.

Optical Materials EXPRESS

References

1. M.E. Fermann, A. Galvanauskas, and G. Sucha, *Ultrafast Lasers: Technology and Applications* (CRC Press, 2002).
2. J. M. Hopkins and W. Sibbett, "Ultrashort pulse lasers: Big payoff in a flash," Sci. Am. **283**(3), 72–79 (2000).
3. J. Kang, C. Kong, P. Feng, X. Wei, Z. C. Luo, E. Y. Lam, and K. K. Y. Wong, "Broadband high-energy all-fiber laser at 1.6 μm," IEEE Photonics Technol. Lett. **30**(4), 311–314 (2018).
4. A. K. Srivastava, S. Radic, C. Wolf, and J. C. Centanni, "Ultradense WDM transmission in L-band," IEEE Photonics Technol. Lett. **12**(11), 1570–1572 (2000).
5. H. Kawagoe, S. Ishida, M. Aramaki, Y. Sakakibara, E. Omoda, H. Kataura, and N. Nishizawa, "Development of a high power supercontinuum source in the 1.7 μm wavelength region for highly penetrative ultrahigh-resolution optical coherence tomography," Biomed. Opt. Express **5**(3), 932–943 (2014).
6. J. Marshall, G. Stewart, and G. Whitenett, "Design of a tunable L-band multi-wavelength laser system for application to gas spectroscopy," Meas. Sci. Technol. **17**(5), 1023–1031 (2006).
7. F. Morin, F. Druon, M. Hanna, and P. Georges, "Microjoule femtosecond fiber laser at 1.6 μm for corneal surgery applications," Opt. Lett. **34**(13), 1991–1993 (2009).
8. P. Cadroas, L. Abdeladim, L. Kotov, M. Likhachev, D. Lipatov, D. Gaponov, A. Hideur, M. Tang, J. Livet, W. Supatto, E. Beaurepaire, and S. Fevrier, "All-fiber femtosecond laser providing 9 nJ, 50 MHz pulses at 1650 nm for three-photon microscopy," J. Opt. **19**(6), 065506 (2017).
9. Y. Ling, Q. Huang, C. Zou, Z. Xing, Z. Yan, C. Zhao, K. Zhou, L. Zhang, and C. Mou, "L-band GHz femtosecond passively harmonic mode-locked Er-doped fiber laser based on nonlinear polarization rotation," IEEE Photonics J. **11**(4), 1–7 (2019).
10. S. M. Park, G. H. Kim, H. D. Lee, and C. S. Kim, "Wavelength-switchable ns-pulsed active mode locking fiber laser for photoacoustic signal generation," Opt. Laser Technol. **115**, 441–446 (2019).
11. O. Okhotnikov, A. Grudinin, and M. Pessa, "Ultra-fast fibre laser systems based on SESAM technology: New horizons and applications," New J. Phys. **6**(1), 177 (2004).
12. A. Martinez, K. Fuse, B. Xu, and S. Yamashita, "Optical deposition of graphene and carbon nanotubes in a fiber ferrule for passive mode-locked lasing," Opt. Express **18**(22), 23054–23061 (2010).
13. K. Kashiwagi and S. Yamashita, "Deposition of carbon nanotubes around microfiber via evanescent light," Opt. Express **17**(20), 18364–18370 (2009).
14. Y. W. Song, S. Yamashita, C. S. Goh, and S. Y. Set, "Carbon nanotube mode lockers with enhanced nonlinearity via evanescent field interaction in D-shaped fibers," Opt. Lett. **32**(2), 148–150 (2007).
15. X. Jiang, W. Li, T. Hai, R. Yue, Z. Chen, C. Lao, and H. Zhang, "Inkjet-printed MXene micro-scale devices for integrated broadband ultrafast photonics," npj 2D Mater. Appl. **3**(1), 1–9 (2019).
16. T. Jiang, K. Yin, C. Wang, J. You, H. Ouyang, R. Miao, C. Zhang, K. Wei, H. Li, H. Chen, R. Zhang, X. Zheng, Z. Xu, X. Cheng, and H. Zhang, "Ultrafast fiber lasers mode-locked by two-dimensional materials: Review and prospect," Photonics Res. **8**(1), 78–90 (2020).
17. M. Yi and Z. Shen, "A review on mechanical exfoliation for the scalable production of graphene," J. Mater. Chem. A **3**(22), 11700–11715 (2015).
18. J. M. Garcia, U. Wurstbauer, A. Levy, L. N. Pfeiffer, A. Pinczuk, A. S. Plaut, L. Wang, C. R. Dean, R. Buizza, V. D. Zande, J. Hone, K. Watanabe, and T. Taniguchi, "Graphene growth on h-BN by molecular beam epitaxy," Solid State Commun. **152**(12), 975–978 (2012).
19. L. Zhang, X. Li, Y. Huang, Y. Ma, X. Wan, and Y. Chen, "Controlled synthesis of few-layered graphene sheets on a large scale using chemical exfoliation," Carbon **48**(8), 2367–2371 (2010).
20. M. Losurdo, M. Giangregorio, P. Capezzuto, and G. Bruno, "Graphene CVD growth on copper and nickel: role of hydrogen in kinetics and structure," Phys. Chem. Chem. Phys. **13**(46), 20836–20843 (2011).
21. H. Zhang, D. Y. Tang, L. M. Zhao, Q. L. Bao, and K. P. Loh, "Large energy mode locking of an erbium-doped fiber laser with atomic layer graphene," Opt. Express **17**(20), 17630–17635 (2009).
22. J. Zhao, Y. Wang, S. Ruan, P. Yan, H. Zhang, Y. H. Tsang, J. Yang, and G. Huang, "Three operation regimes with an L-band ultrafast fiber laser passively mode-locked by graphene oxide saturable absorber," J. Opt. Soc. Am. B **31**(4), 716–722 (2014).
23. R. Wang, Y. Liu, M. Jiang, X. Xu, H. Wu, Y. Tian, J. Bai, and Z. Ren, "Passively Q-switched and mode-locked fiber laser research based on graphene saturable absorbers," Opt. Quantum Electron. **49**(4), 137 (2017).
24. X. M. Liu, H. R. Yang, Y. D. Cui, G. W. Chen, Y. Yang, X. Q. Wu, X. K. Yao, D. D. Han, X. X. Han, C. Zeng, J. Guo, W. L. Li, G. Cheng, and L. M. Tong, "Graphene-clad microfibre saturable absorber for ultrafast fibre lasers," Sci. Rep. **6**(1), 26024 (2016).
25. A. A. Nafiey, A. Addad, B. Sieber, G. Chastanet, A. Barras, S. Szunerits, and R. Boukherroub, "Reduced graphene oxide decorated with Co_3O_4 nanoparticles (rGO-Co_3O_4) nanocomposite: a reusable catalyst for highly efficient reduction of 4-nitrophenol, and Cr (VI) and dye removal from aqueous solutions," Chem. Eng. J. **322**, 375–384 (2017).
26. E. K. Ng, K. Y. Lau, H. K. Lee, M. H. Abu Bakar, Y. Mustapha Kamil, M. F. Omar, and M. A. Mahdi, "Saturable absorber incorporating graphene oxide polymer composite through dip coating for mode-locked fiber laser," Opt. Mater. **100**, 109619 (2020).

Optical Materials EXPRESS

27. Y. Chen, C. Zhao, S. Chen, J. Du, P. Tang, G. Jiang, H. Zhang, S. Wen, and D. Tang, "Large energy, wavelength widely tunable, topological insulator Q-switched erbium-doped fiber laser," IEEE J. Sel. Top. Quantum Electron. **20**(5), 317–322 (2014).
28. Q. Sheng, M. Feng, W. Xin, T. Han, Y. Liu, Z. Liu, and J. Tian, "Actively manipulation of operation states in passively pulsed fiber lasers by using graphene saturable absorber on microfiber," Opt. Express **21**(12), 14859–14866 (2013).
29. Z. Sun, T. Hasan, F. Torrisi, D. Popa, G. Privitera, F. Wang, F. Bonaccorso, D. M. Basko, and A. C. Ferarri, "Graphene mode-locked ultrafast laser," ACS Nano **4**(2), 803–810 (2010).
30. W. Xin, Z. B. Liu, Q. W. Sheng, M. Feng, L. G. Huang, P. Wang, W. S. Jiang, F. Xing, Y. G. Liu, and J. G. Tian, "Flexible graphene saturable absorber on two-layer structure for tunable mode-locked soliton fiber laser," Opt. Express **22**(9), 10239–10247 (2014).
31. X. Jiang, S. Gross, H. Zhang, Z. Guo, M. J. Withford, and A. Fuerbach, "Bismuth telluride topological insulator nanosheet saturable absorbers for q-switched mode-locked Tm: ZBLAN waveguide lasers," Ann. Phys. **528**(7-8), 543–550 (2016).
32. X. Jiang, S. Gross, M. J. Withford, H. Zhang, D.-I. Yeom, F. Rotermund, and A. Fuerbach, "Low-dimensional nanomaterial saturable absorbers for ultrashort-pulsed waveguide lasers," Opt. Mater. Express **8**(10), 3055–3071 (2018).
33. M. W. Wright, H. Yao, and J. R. Marciante, "Resonant pumping of Er-doped fiber amplifiers for improved laser efficiency in free-space optical communications," IPN Progress Report, 42–189 (2012).
34. D. H. Lee, H. H. Lee, J. M. Oh, and B. J. Kim, "Investigation of amplifying mechanism in an L-band erbium-doped fiber amplifier pumped by a 980 nm pump," J. Opt. Soc. Korea **7**(2), 67–71 (2003).
35. H. Xia, H. Li, C. Lan, C. Li, X. Zhang, S. Zhang, and Y. Liu, "Ultrafast erbium-doped fiber laser mode-locked by a CVD-grown molybdenum disulfide (MoS_2) saturable absorber," Opt. Express **22**(14), 17341–17348 (2014).
36. W. Du, H. Li, C. Lan, C. Li, J. Li, Z. Wang, and Y. Liu, "Graphene/WS_2 heterostructure saturable absorbers for ultrashort pulse generation in L-band passively mode-locked fiber lasers,'," Opt. Express **28**(8), 11514–11523 (2020).
37. B. Guo, Q. Lyu, Y. Yao, and P. Wang, "Direct generation of dip-type sidebands from WS_2 mode-locked fiber laser," Opt. Mater. Express **6**(8), 2475–2486 (2016).
38. T. Kolokolnikov, M. Nizette, T. Erneux, N. Joly, and S. Bielawski, "The Q-switching instability in passively mode-locked lasers," Phys. D **219**(1), 13–21 (2006).
39. D. Steinberg, R. M. Gerosa, F. N. Pellicer, J. D. Zapata, S. H. Domingues, E. A. T. de Souza, and L. A. Saito, "Graphene oxide and reduced graphene oxide as saturable absorbers onto D-shaped fibers for sub 200-fs EDFL mode-locking," Opt. Mater. Express **8**(1), 144–156 (2018).
40. Z. D. Chen, Y. G. Wang, L. Li, R. D. Lv, L. L. Wei, S. C. Liu, and X. Wang, "Reduced graphene oxide as saturable absorbers for erbium-doped passively mode-locked fiber laser," Chin. Phys. B **27**(8), 084206 (2018).